International Journal of Humanoid Robotics
Vol. 13, No. 3 (2016) 1650009 (24 pages)
© World Scientific Publishing Company
DOI: 10.1142/S0219843616500092

A Comparative Study for Postural Synergy Synthesis Using Linear and Nonlinear Methods

Kai Xu*, Huan Liu† and Yuheng Du‡

UM-SJTU Joint Institute, Shanghai Jiao Tong University,
800 Dongchuan Rd, Shanghai 200240, P. R. China
**k.xu@sjtu.edu.cn*
†liuhuan_2013@sjtu.edu.cn
‡jhdyh1991@sjtu.edu.cn

Xiangyang Zhu

School of Mechanical Engineering,
Shanghai Jiao Tong University,
800 Dongchuan Rd, Shanghai 200240, P. R. China
mexyzhu@sjtu.edu.cn

Received 9 February 2015
Accepted 5 January 2016
Published

Human controls dozens of muscles for different hand postures in a coordinated manner. Such coordination is referred to as a postural synergy. Postural synergy has enabled an anthropomorphic robotic hand with many actuators to be applied as a prosthetic hand and controlled by two to three channels of biological signals. Principle component analysis (PCA) of the hand postures has become a popular way to extract the postural synergies. However, relatively big errors are often produced while the hand postures are reconstructed using these PCA-synthesized synergies due to the linearity nature of this method. This paper presents a comparative study in which the postural synergies are synthesized using both linear and nonlinear methods. Specifically, the Gaussian process (GP) latent variable model (GPLVM), as a nonlinear dimension reduction method, is implemented to produce nonlinear postural synergies and the hand postures can then be reconstructed from the two-dimensional synergy plane. Computational and experimental verifications show that the posture reconstruction errors are greatly reduced using this nonlinear method. The results suggest that the use of nonlinear postural synergies should be considered while applying a dexterous robotic hand as prosthesis. Versatile hand postures could be formed via only two channels of bio-signals.

Keywords: Postural synergy; grasping; prosthetic hand; Gaussian process latent variable model; principle component analysis.

1. Introduction

Efforts have been continuously made to improve the construction of an anthropomorphic prosthetic hand. Such a hand is expected to be versatile for daily tasks and

controllable through a low-bandwidth bio-signal interface, such as electro-myography (EMG) or electro-encephalography (EEG). The paradox between hand dexterity and control simplicity was recently tackled utilizing the concept of postural synergy.

Postural synergy originally refers to the coupled flexion and/or extension of a group of muscles.[1] Human central nervous system (CNS) controls dozens of hand muscles for different postures through combining several postural synergies. Combination of two primary postural synergies accounts for about 84% of the variance of many grasping postures.[2]

The postural synergy provides a continuous interpretation of hand motion atlas that was previously described by discrete grasp taxonomy.[3–6] Dexterous control of a multi-degree of freedom (DoF) robotic hand (e.g., the existing state-of-the-art ones[7–9]) could be conveniently achieved via two to three postural synergies. Using two to three sensors (e.g., EMG sensors) to sense an amputee's intention and provide inputs to the postural synergies, the aforementioned multi-DoF robotic hands could be applied as prostheses. Several designs have demonstrated this idea, such as the DLR II Hand,[10] the SAH hand,[11] the UB hand,[12] the ACT hand,[13,14] the First Hand[15] and the DEXMART hand[16] with two to three synergies for the control of 12 to 24 actuators.

When two to three postural synergies are used to control dozens of actuators, the synergies are implemented digitally in the controller. It is also possible to implement the postural synergies mechanically. Namely the motion inputs from two actuators are transferred to all the hand joints through a complicated mechanical transmission unit. Such a mechanical implementation of the postural synergy has been realized using differential pulleys,[17–20] planetary gears[21,22] and continuum mechanisms.[23] These mechanical synergy-based designs enriched the designs of underactuated prosthetic hands, such as the existing state-of-the-art ones.[24–27]

The postural synergies are usually extracted from a set of hand postures using the principle component analysis (PCA) and then implemented digitally or mechanically. These linear postural synergies are also referred to as eigengrasps or eigenpostures.[28,29] Due to the linearity nature of this method, reconstruction errors are often relatively big when the first two to three postural synergies are used to reproduce a grasp, since people often use five to six postural synergies for grasp formations and fine posture adjustments. Although it is possible to optimize the synergy inputs to form stable grasps of various objects using two postural synergies,[29] it is still worth exploring alternative methods that encode more posture information in a two-dimensional synergy space.

Gaussian process latent variable model (GPLVM), as a nonlinear method of dimension reduction, was recently used to quantitatively evaluate a human hand's motion capability[30] as well as plan a grasp.[31] Inspired by these results, this paper proposes to apply the GPLVM method to synthesize nonlinear postural synergies for the control of a multi-DoF prosthetic hand. The method is then compared to the PCA-based linear method to demonstrate the effectiveness of both methods.

AQ: We have provided short title. Please approve.

The positions and orientations of the finger tips were recorded as the observed data in the published studies,[30,31] but this paper proposes to use the joint values as the observed data due to their direct correspondence in realizing hand postures.

Contributions of this paper mainly lie on the simulative and experimental examinations of hand pose reconstruction errors via the postural synergies generated using the PCA-based linear method and the GPLVM-based nonlinear method. Minor contributions also include the setup of a 13-DoF anthropomorphic prosthetic hand and the collection of a comprehensive set of hand postures (not only grasps but also hand postures for gesture signs). The results suggest that the use of nonlinear postural synergies should be considered while applying a multi-DoF dexterous robotic hand as prosthesis, since versatile hand postures could be reconstructed more precisely via only two channels of bio-signals.

The paper is organized as follows. Section 2 presents the construction of the 13-DoF prosthetic hand and the collection of hand postures. Postural synergy synthesis using the PCA-based linear method and the GPLVM-based nonlinear method is presented in Sec. 3. Section 4 reports the numerical and actual experiments that compare the reconstruction errors of the hand postures that are reproduced using the linear and the nonlinear postural synergies. Conclusions are then summarized in Sec. 5.

2. Construction of a 13-DoF Prosthetic Hand and Collection of the Postures

An anthropomorphic prosthetic hand was designed and constructed as shown in Fig. 1(a). The joints are denoted as follows. Letters T, I, M, R and L before the underscore indicate the joints for the thumb, the index, the middle, the ring and the little fingers, respectively. Abbreviations of *rot*, *mcp*, *ip*, *abd*, *pip* and *dip* after

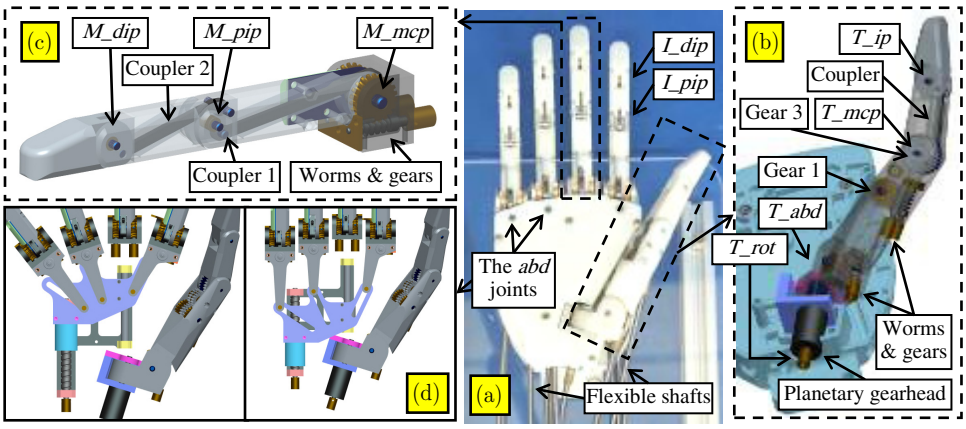

Fig. 1. Construction of the anthropomorphic prosthetic hand: (a) joint arrangements, (b) structure of the thumb, (c) structures of the fingers and (d) structure of the *abd* joints.

the underscore indicate the rotation, the metacarpophalangeal, the interphalangeal, the abduction, the proximal and the distal interphalangeal joints, respectively.

In total the hand has 19 joints: the *T_ip*, *T_mcp*, *T_abd* and *T_rot* joints for the thumb; the *dip*, *pip* and *mcp* joints for the four fingers; and the *abd* joints for the index, the ring and the little fingers.

For all the *ip* joints (including the *dip* and *pip* joints) and the *mcp* joints, zero values are defined as they reach their full extensions whereas positive values are defined for flexion motions. For all the *abd* joints, positive values are defined in their abduction motions. Positive value of the *T_rot* joint is defined in its opposition motion. Motion ranges of the hand joints are then summarized in Table 1.

The prosthetic hand itself in Fig. 1 was also used in a previous study[22] for mechanical posture synergies. As shown in Fig. 2(b), 13 miniature servomotors are used and programmed here to drive the hand so as to form the experimental setup in this paper. The construction of the hand is hence only briefly summarized. The actuation scheme of the thumb is shown in Fig. 1(b). A flexible shaft is connected to a planetary gearhead (with a gear ratio of 18.17:1) to drive the *T_rot* joint. Another flexible shaft is connected to a worm to drive a worm gear and then the *T_abd* joint. Two more flexible shafts are connected to two pairs of worms and gears to drive the *T_mcp* and the *T_ip* joints via two gear trains and a coupler. The gear (Gear 3) has 28 teeth whereas the pinion (Gear 1) has 18 teeth with a module of 0.5. An idler gear was added to change the rotation direction of Gear 3. Gear 1 is attached to the worm gear. Gear 3 is attached to the thumb's proximal phalanx to drive the *T_mcp* joint or to a coupler to drive the *T_ip* joint. All worms and gears in the hand have a gear ratio of 20:1.

Since the actuation of the index, the middle, the ring and the little fingers is similar, only the structure of the middle finger is shown in Fig. 1(c). Two flexible shafts are connected to two pairs of worms and gears. One worm gear is attached to the proximal phalanx to drive the *M_mcp* joint. The other worm gear is attached to Coupler 1 and Coupler 2 to drive the *M_pip* and the *M_dip* joints. Similar designs could be found in Ref. 32. The coupling between the *M_pip* and the *M_dip* joints is close to 1:1. As shown in Fig. 1(d), a plate cam is translated to realize coupled abduction motions of the index, the ring and the little fingers. The cam is actuated by a miniature ball screw with a diameter of 6 mm and a lead of 2 mm. Motion axes of the *abd* joints intersect with those of the *mcp* joints.

Thirteen miniature servomotors are connected to 13 flexible shafts to drive the hand, as shown in Fig. 2(a). The motors are Maxon A-max 16 (1.2 watts) with gearhead (GP 16A, 29:1) and encoders (MEnc 13, 16 CPT). The servomotors are controlled under a real-time operating system generated by the xPC module of MATLAB. Other control hardwares include the LSC 30/2 amplifiers (Maxon), the PCL727 D/A cards (AdvanTech), the CNT32-8M counter cards (ConTec) and an Intel x86 platform workstation.

Hand movements are commanded in the hand's actuator space. A desktop PC is used to generate the actuator trajectories and the trajectories are sent to the control workstation via user datagram protocol (UDP) for execution.

Table 1. Motion ranges and joint angles of the hand under various postures.

Joints	Joint ranges (°)	Posture Set-1 (°)									Set-2 (°)						Set-3 (°)		
		P1	P2	P3	P4	P5	P6	P7	P8	P9	P10	P11	P12	P13	P14	P15	P16	P17	P18
T_rot	[0, 90]	58	81	35	70	59	50	85	56	25	48	44	37	65	87	69	80	90	10
T_mcp	[0, 90]	30	31	25	40	38	31	25	46	55	24	36	42	45	50	35	40	55	0
T_ip	[0, 90]	20	27	24	20	43	36	40	43	35	29	40	50	50	55	40	30	55	0
T_abd	[0, 70]	65	65	42	65	60	40	60	42	40	30	38	43	52	55	40	40	45	40
I_mcp	[0, 90]	25	21	40	30	50	40	42	53	80	45	58	75	50	25	16	0	0	90
M_mcp	[0, 90]	22	38	56	40	60	55	56	56	78	55	43	45	1	4	21	80	0	90
R_mcp	[0, 90]	23	44	62	43	60	54	59	58	72	55	50	41	0	17	52	85	85	90
L_mcp	[0, 90]	34	51	71	54	58	49	65	61	70	55	50	73	50	55	55	90	90	20
I_pip	[0, 100]	40	32	70	40	54	57	59	62	80	59	54	52	55	53	56	0	0	90
M_pip	[0, 100]	54	44	85	45	50	75	56	66	79	63	85	69	77	69	69	90	0	90
R_pip	[0, 100]	55	43	84	55	55	75	53	70	74	75	69	70	72	73	76	90	90	90
L_pip	[0, 100]	48	39	80	50	69	74	59	71	71	71	65	57	80	69	78	90	90	0
I_abd	[0, 20]	10	8	7	10	9	10	14	13	8	5	10	10	5	5	17	5	10	10

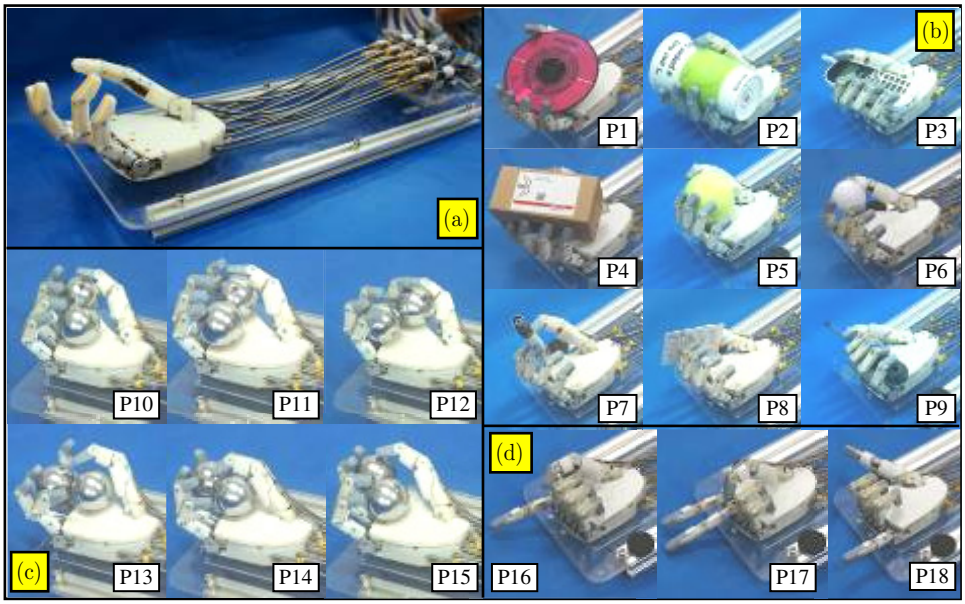

Fig. 2. Collections hand postures: (a) the prosthetic hand, (b) grasping postures for daily-life objects, (c) in-hand manipulating postures of two balls and (d) sign gestures; the postures are designated consistently with those in Table 1.

The hand was then commanded for various postures and signs as shown in Fig. 2. Three sets of hand postures were collected.

- The first set (Set-1) consists of the grasping postures for 15 daily-life objects, including 1. a CD, 2. a cup, 3. a coca can, 4. a spray can, 5. a phone, 6. a flat bottle, 7. a box, 8. a book, 9. a tennis ball, 10. a jar, 11. a golf ball, 12. a drug bottle, 13. a pen, 14. a credit card and 15. a screwdriver. The posture #14 is similar to the grasp for a key while the posture #15 is similar to the grasp for a tooth brush. The set is partially shown in Fig. 2(b).
- The second set (Set-2) includes six key postures for an in-hand manipulation task. The proposed manipulation paradigm is to rotate two rehabilitation training balls as shown in Fig. 2(c). This exercise could help maintain or recover hand motor functions. It might seem worthless for amputees but the motivation here is to simply use this example to verify the effectiveness of synergy-based control for dissimilar hand postures. This ball-rotating motion was achieved via using these six postures with mechanical postural synergies in a previous study.[22]
- The third set (Set-3) includes 10 gesture signs, including 1. one, 2. two, 3. three, 4. four, 5. five, 6. six, 7. seven, 8. eight, 9. nine and 10. zero. The set is partially shown in Fig. 2(d). The gesture P16 designates "one", while the gesture P17 designates "two" and the gesture P18 designates "six". This set consists of hand postures often with the joints at the upper or lower limits.

The motivation of collecting the three sets of hand postures is to gradually reveal the motion capabilities of a human hand.

The first set only fulfills basic daily needs of an amputee. A healthy human hand has motion capabilities way beyond these grasping postures. As shown in previous studies[2,33] and demonstrated by the experiments in Sec. 4.1, these postures in the Set-1 can be reproduced adequately using two linear postural synergies.

The second set is an example of in-hand manipulation. Hand postures for grasping and in-hand manipulation could be considered dissimilar in a sense that the postural synergies extracted from Set-2 cannot effectively reproduce grasps for daily-life objects.[22] A human hand certainly is capable for many different in-hand manipulation tasks. It will be shown later in this paper that even the inclusion of one set of such dissimilar postures will prevent hand postures from being effectively reproduced by two linear postural synergies.

The third set shows additional examples of a human hand's motion capabilities. Nonlinear postural synergies could regenerate these postures much better than the linear postural synergies under the same synergy dimensions.

Motion ranges and joint angles of the hand under various hand postures are summarized in Table 1. The postures are designated consistently in Fig. 2 and Table 1. Table 1 only shows the *I_abd* joint angle since the *R_abd* and the *L_abd* joint angles are coupled to that of the *I_abd* joint due to the coupling as shown in Fig. 1(d).

3. Postural Synergy Synthesis

With the hand postures collected as in Sec. 2, this section presents a linear and a nonlinear method for the postural synergy synthesis.

Postural synergy synthesis was directly carried out from the postures of the prosthetic hand from Fig. 2. This approach avoids the unnecessarily complex procedures of recording and analyzing human hand motions using a complicated system (e.g., CyberGlove^{TM}). It provides direct posture results for synergy synthesis. Similar approaches could be found in previous studies.[10,22]

As mentioned in Sec. 2, the prosthetic hand is driven by 13 servomotors. The hand posture space (it is also referred to as the observed data space) is hence a thirteen-dimensional one. Specifically, Sec. 3.1 presents the PCA-based linear method for postural synergy synthesis where the posture space is reduced to a two-dimensional linear synergy space. Section 3.2 presents the GPLVM-based nonlinear method to reduce the posture space (the data space) to a two-dimensional latent space. The lower-dimensional spaces (namely the synergy space and the latent space) are called differently to differentiate one from the other.

3.1. *Synthesis via linear dimension reduction*

The PCA-based linear method for the postural synergy synthesis essentially applies singular value decomposition (SVD) to a posture matrix assembled from the observed data to extract a set of principal components as the postural synergies.

For N observed hand postures, let D denote the dimension of the data space which is the number of independent joint angles of the prosthetic hand. Then a posture matrix $\mathbf{J}$ could be formed by putting the hand posture vectors side by side.

$$\mathbf{J} = [\mathbf{j}_1 \quad \mathbf{j}_2 \quad \cdots \quad \mathbf{j}_N] \in \Re^{D\times N}, \tag{1}$$

where $\mathbf{j} \in \Re^{D\times 1}$ is a hand posture vector. D is 13 due to the fact that 13 independent servomotor inputs are needed to drive the prosthetic hand. Representative values of $\mathbf{j}$ could be seen as columns in Table 1. In the rest of this paper, hand postures will all be expressed using the joint angles, in order to avoid complicating the paper with the transmission ratios in the worm and gears, planetary gears, ball screws, etc.

Applying SVD to the posture matrix leads to the results below.

$$\begin{aligned}\mathbf{J} &= \bar{\mathbf{J}} + \mathbf{U}_{D\times D}\mathbf{\Sigma}_{D\times N}\mathbf{V}_{N\times N}^T \\ &= \bar{\mathbf{J}} + [\mathbf{u}_1 \quad \mathbf{u}_2 \quad \cdots \quad \mathbf{u}_D][\mathrm{diag}(\delta_1, \delta_2, \ldots, \delta_D) \quad \mathbf{0}]\begin{bmatrix}\mathbf{v}_1^T \\ \mathbf{v}_2^T \\ \vdots \\ \mathbf{v}_N^T\end{bmatrix},\end{aligned} \tag{2}$$

where $\bar{\mathbf{J}} = [\bar{\mathbf{j}} \quad \bar{\mathbf{j}} \quad \cdots \quad \bar{\mathbf{j}}]$ is the average posture matrix and $\bar{\mathbf{j}}$ corresponds to a posture that all the joints in the hand are at the middle points of their motion ranges.

If the singular values δ_m $(m \geq 3)$ are neglected, the posture matrix can be approximated as in Eq. (3) such that each hand posture can be approximated as in Eq. (4).

$$\tilde{\mathbf{J}} = \bar{\mathbf{J}} + [\mathbf{u}_1 \quad \mathbf{u}_2]\begin{bmatrix}\delta_1\mathbf{v}_1^T \\ \delta_2\mathbf{v}_2^T\end{bmatrix} = \bar{\mathbf{J}} + [\mathbf{u}_1 \quad \mathbf{u}_2]\mathbf{Q}, \tag{3}$$

where $\mathbf{Q} = \begin{bmatrix} q_{11} & q_{12} & \cdots & q_{1N} \\ q_{21} & q_{22} & \cdots & q_{2N}\end{bmatrix} \in \Re^{2\times N}$ is the matrix of the synergy inputs.

$$\tilde{\mathbf{j}}_i = \bar{\mathbf{j}} + q_{1i}\mathbf{u}_1 + q_{2i}\mathbf{u}_2, \quad i = 1, 2, \ldots, N. \tag{4}$$

Vectors $\mathbf{u}_1$ and $\mathbf{u}_2$ are hence referred to as the postural synergies, while q_{1i} and q_{2i} are the synergy inputs. These postural synergies are also referred to as eigengrasps or eigenpostures.[28,29] They are actually two linear bases of the hand posture space. Via this linear method of dimension reduction, the posture matrix $\mathbf{J} \in \Re^{13\times N}$ is mapped to the synergy matrix $\mathbf{Q} \in \Re^{2\times N}$. Now, various hand postures could be formed by linearly combining the two postural synergies.

Obviously there are joint errors when a hand posture is reproduced using the postural synergies. Posture error vectors can then be defined as below

$$\mathbf{j}_i^{\mathrm{err}} = \mathbf{j}_i - \tilde{\mathbf{j}}_i, \quad i = 1, 2, \ldots, N. \tag{5}$$

3.2. *Synthesis via nonlinear dimension reduction*

The PCA-based linear method for the postural synergy synthesis is effective in dealing with similar hand postures (e.g., the postures in Set-1). When dissimilar hand postures are included, such a linear method becomes less sufficient. This section presents a nonlinear method for the synergy synthesis. The experimental results in Sec. 4 would show the effectiveness of this nonlinear method.

3.2.1. *Gaussian process latent variable models*

The nonlinear method for the synergy synthesis is essentially a nonlinear dimension reduction technique that reduces the dimension of the hand posture space from 13 to 2. The adopted nonlinear method is the GPLVM due to its proven effectiveness for similar problems in previous studies.[30,34]

For N hand postures, the posture matrix $\mathbf{J} \in \Re^{D\times N}$ from Eq. (1) is still used for the sake of consistency. A latent matrix $\mathbf{X} = [\mathbf{x}_1 \quad \mathbf{x}_2 \quad \cdots \quad \mathbf{x}_N] \in \Re^{2\times N}$ is expected after the nonlinear dimension reduction. A different symbol $\mathbf{X}$ for the latent matrix is used to differentiate the synergy matrix $\mathbf{Q}$ from the results obtained using the linear method. A hand posture $\mathbf{j}_i \in \Re^{D\times 1}$ could then be represented by the latent vector $\mathbf{x}_i \in \Re^{2\times 1}$ in the latent space $\mathbf{x}_i \xrightarrow{f} \mathbf{j}_i$.

The basic idea is to use GPLVM to construct a nonlinear mapping f as in Eq. (6).

$$\mathbf{j}_i = \bar{\mathbf{j}} + f(\mathbf{x}_i) + \varepsilon, \tag{6}$$

where $\bar{\mathbf{j}} = \frac{1}{N}\sum_{i=1}^{N}\mathbf{j}_i$ is the average posture vector and $\varepsilon \sim N(\mathbf{0}, \theta_{\text{white}}\mathbf{I})$ is an item for additive Gaussian noise.

The generative mapping f is assumed to be a Gaussian process (GP) prior. A different definition of the average posture $\bar{\mathbf{j}}$ is used here because the GP is assumed to have a zero mean function. Hence the derivation below mainly deals with the covariance function.

Then the likelihood of the centered posture matrix $\overleftrightarrow{\mathbf{j}} = \mathbf{J} - \bar{\mathbf{J}}$ with respect to the mapping could be formulated as in Eq. (7). Since the structure of the mapping is unknown, the mapping f should be marginalized for the marginal likelihood as in Eq. (8). According to the derivations detailed in previous studies,[34] Eq. (8) could be integrated to an explicit form as in Eq. (9).

$$p(\overleftrightarrow{\mathbf{J}}\,|f, \theta_{\text{white}}) = \prod_{i=1}^{N} N(\overleftrightarrow{\mathbf{j}}_i|f, \theta_{\text{white}}), \tag{7}$$

$$p(\overset{t}{\mathbf{J}}) = \int p(\overset{t}{\mathbf{J}}\,|f)p(f)\,df, \tag{8}$$

$$p(\overleftrightarrow{\mathbf{J}}) = \prod_{m=1}^{D} \frac{1}{(2\pi)^{N/2}|\mathbf{K}|^{1/2}}\, e^{-\frac{1}{2}\vec{\mathbf{j}}_m\mathbf{K}^{-1}\vec{\mathbf{j}}_m^{\,T}}, \tag{9}$$

where $\overleftrightarrow{\mathbf{j}}_i = \mathbf{j}_i - \bar{\mathbf{j}}$ is a centered posture vector and $\vec{\mathbf{j}}_m \in \Re^{1\times N}$ is the mth row of the centered posture matrix $\overleftrightarrow{\mathbf{J}}_i$.

The probability in Eq. (9) is calculated as the product of D independent GP. Each GP is responsible for one dimension of the hand posture space (data space). The covariance matrix $\mathbf{K} \in \Re^{N\times N}$ in Eq. (9) adopts the form of a radial basis function (RBF) kernel with bias θ_{bias} and white noise θ_{white}. Its element in the mth row and nth column is given by Eq. (10).

$$k(\mathbf{x}_m, \mathbf{x}_n) = \theta_r e^{-\frac{1}{2}\gamma_r(\mathbf{x}_m-\mathbf{x}_n)^T(\mathbf{x}_m-\mathbf{x}_n)} + \theta_{\text{bias}} + \theta_{\text{white}}\delta_{\text{mn}}, \tag{10}$$

where δ_{mn} is the Kronecker delta function.

The marginal likelihood $p(\overleftrightarrow{\mathbf{J}})$ as in Eq. (9) shall be maximized to find $\mathbf{x}_i$ in $\mathbf{X}$ and the parameters (θ_r, γ_r, θ_{bias} and θ_{white}) of the covariance function $k(\mathbf{x}_m, \mathbf{x}_n)$.

3.2.2. *Back constraints*

It is desired for a nonlinear mapping to preserve the locality. Namely, nearby points in the data space are expected to remain close in the latent space. However, the optimization of the marginal likelihood $p(\overleftrightarrow{\mathbf{J}})$ from Eq. (9) does not guarantee the locality even though it does generate a smooth mapping.

It is possible to introduce some modifications to the formulation to preserve the locality and this is referred to as a back-constrained GPLVM method.[35] The modification involves replacing the elements of the latent matrix $\mathbf{X}$ as in Eq. (11), where $k_{bc}(\mathbf{j}_n, \mathbf{j}_t)$ is the back-constraint kernel and it has an RBF form as in Eq. (12). The parameter γ_{bc} is for the kernel width and it affects how well the locality is to be preserved.

$$x_{mn} = \sum_{t=1}^{N} a_{mt} k_{bc}(\mathbf{j}_n, \mathbf{j}_t), \tag{11}$$

$$k_{bc}(\mathbf{j}_m, \mathbf{j}_n) = e^{-\frac{1}{2}\gamma_{bc}(\mathbf{j}_m-\mathbf{j}_n)^T(\mathbf{j}_m-\mathbf{j}_n)}. \tag{12}$$

In this back-constrained GPLVM formulation, the marginal likelihood $p(\overleftrightarrow{\mathbf{J}})$ as in Eq. (9) is to be maximized with respect to the coefficients a_{mt} as in Eq. (11). When the maximization terminates, the latent matrix $\mathbf{X}$ would be obtained according to Eq. (11).

3.2.3. *Implementation and visualization*

Unlike the straightforward implementation of the linear method, the implementation and the visualization of this nonlinear GPLVM method might need a bit more elaboration.

Given the posture matrix $\mathbf{J} \in \Re^{D\times N}$ and with the back-constrained GPLVM procedure implemented, the marginal likelihood $p(\overleftrightarrow{\mathbf{J}})$ as in Eq. (9) is maximized with respect to the coefficients a_{mt} ($m = 1, 2$ and $t = 1, 2, \ldots, N$) with the parameters initialized at $\theta_r = \gamma_r = 1$ and $\theta_{\text{bias}} = \theta_{\text{white}} = e^{-1}$. When the maximization terminates, the latent variable $\mathbf{x}_i$ in $\mathbf{X}$ would be obtained according to Eq. (11).

The parameters (θ_r, γ_r, θ_{bias}, θ_{white} and γ_{bc}) are for the covariance functions $k(\mathbf{x}_m, \mathbf{x}_n)$ and $k_{bc}(\mathbf{j}_m, \mathbf{j}_n)$ as in Eqs. (10) and (12), respectively. The parameters of θ_r, γ_r, θ_{bias} and θ_{white} are to be optimized. Different γ_{bc} values would lead to different optimization results (e.g., different values of these coefficients a_{mt} and the latent variables $\mathbf{x}_i$). However, since the latent variables do not have explicit physical meanings, the latent variables $\mathbf{x}_i$ obtained under different γ_{bc} values are equally good in visualizing the high-dimensional data in the low-dimensional latent space. The parameter is hence set so as $\gamma_{bc} = 0.001$ without loss of generality, as long as the results maintain proper locality.

The scaled conjugate gradient optimization algorithm[36] was used to obtain the maxima of the marginal likelihood $p(\overleftrightarrow{\mathbf{J}})$. The number of iterations is set to 500 when the algorithm was implemented in MATLAB.

AQ: Figure 4 is cited before fig. 3. Please check citation.

On the latent plane as shown in Fig. 4, any point $\mathbf{x}_*$ in the latent space (even for the points $\mathbf{x}_i$ obtained from the maximization of the marginal likelihood) could be mapped to a point $\mathbf{j}_*$ in the hand posture space (data space) as in Eq. (13).

$$\mathbf{j}_* = \bar{\mathbf{j}} + \overleftrightarrow{\mathbf{J}}\,\mathbf{K}^{-1}\mathbf{k}_*, \tag{13}$$

where $\mathbf{K}$ is the covariance matrix as in Eq. (9) generated using the latent variables $\mathbf{x}_i$; $\mathbf{k}_* \in \Re^{N\times 1}$ is a vector of covariance as in Eq. (14) with $k(\mathbf{x}_i, \mathbf{x}_*)$ specified according to Eq. (10).

$$\mathbf{k}_* = [k(\mathbf{x}_1, \mathbf{x}_*) \quad k(\mathbf{x}_2, \mathbf{x}_*) \quad \cdots \quad k(\mathbf{x}_n, \mathbf{x}_*)]^T. \tag{14}$$

Even with the nonlinear postural synergies, the original hand postures $\mathbf{j}_i$ are still reproduced with some errors that could be quantified as in Eq. (15).

$$\mathbf{j}_i^{\text{err}} = \mathbf{j}_i - \mathbf{j}_*(\mathbf{x}_i), \quad i = 1, 2, \ldots, N, \tag{15}$$

where $\mathbf{j}_*(\mathbf{x}_i)$ is obtained according to Eq. (13) using $\mathbf{x}_i$ for $\mathbf{x}_*$.

Each point $\mathbf{x}_*$ in the latent place is correlated to the latent points $\mathbf{x}_i$ obtained from the maximization of the marginal likelihood. The variance which could be calculated according to Eq. (16) is hence visualized as the point's gray scale as in Fig. 4.

$$\sigma_*^2 = k(\mathbf{x}_*, \mathbf{x}_*) - \mathbf{k}_*^T\mathbf{K}^{-1}\mathbf{k}_*, \tag{16}$$

where $k(\mathbf{x}_*, \mathbf{x}_*)$ is calculated using Eq. (10).

4. Numerical and Experimental Reconstruction of the Hand Postures

With the linear and the nonlinear methods for postural synergy synthesis formulated in Sec. 3, this section demonstrates the effectiveness of these methods through numerical simulations and experimental verifications.

4.1. *Numerical reconstruction of hand postures*

When the posture synergies are synthesized using the linear method, SVD is applied to the posture matrix $\mathbf{J}$ and 13 ($D = 13$) singular values are obtained.

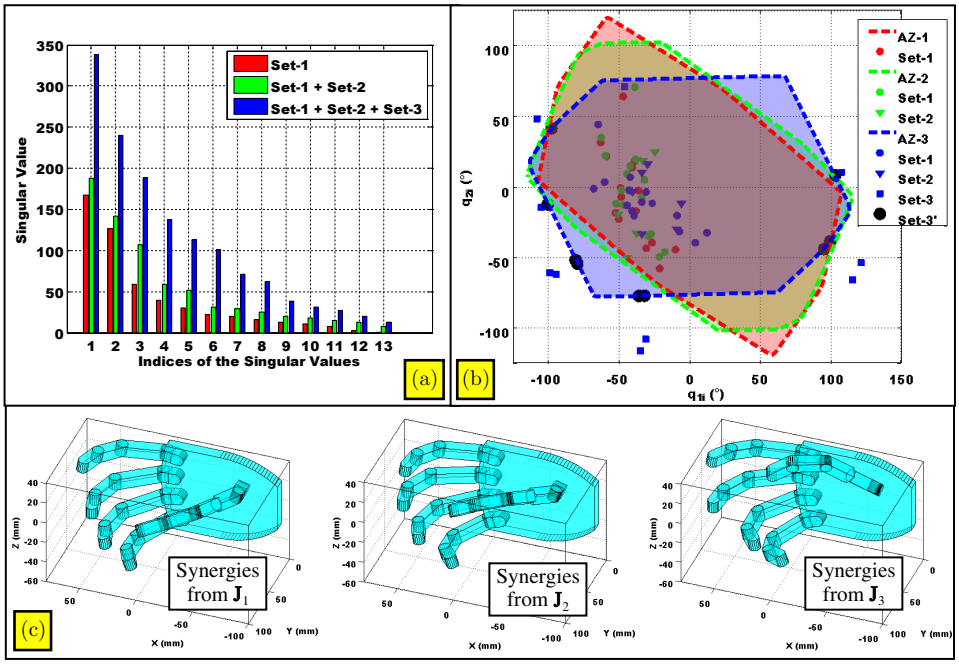

Fig. 3. Postural synergy synthesis using the linear method: (a) singular values, (b) actuation zones and (c) reproduced postures for cup grasping.

The thirteen-dimensional hand posture space is then reduced to the two-dimensional synergy space by neglecting the singular values δ_m $(m \geq 3)$, as shown in Eq. (3). This approximation is acceptable as long as the biggest two singular values are substantially larger than the others.

When a posture matrix $\mathbf{J}_1$ is formed using the 15 hand postures from the Set-1, all the singular values can be obtained and they are plotted in Fig. 3(a). The biggest two singular values are 167.02 and 126.80, whereas the third biggest singular value is only 58.80. The variance ratio η, which is defined as the ratio of the squared sum of the first two singular values over the squared sum of all the singular values as in Eq. (17), is 85.57%.

$$\eta = \frac{\delta_1^2 + \delta_2^2}{\sum_{m=1}^{D} \delta_m^2}. \tag{17}$$

The two vectors $\mathbf{u}_1$ and $\mathbf{u}_2$, which are associated with the biggest two singular values, are referred to as the postural synergies. When the synergy inputs q_{1i} and q_{2i} are varied continuously, different hand postures can be generated according to Eq. (4). While the synergy inputs are varied, none of the hand joint angles should exceed the joint limits as listed in Table 1. For the synergy pair $\mathbf{u}_1$ and $\mathbf{u}_2$ generated from $\mathbf{J}_1$, an actuation zone (AZ-1) could be found by enumerating the synergy inputs and

examining whether a generated hand posture violates the hand joint limits, as shown in Fig. 3(b).

Using the postural synergies ($\mathbf{u}_1$ and $\mathbf{u}_2$) extracted from $\mathbf{J}_1$, the hand postures in the Set-1 could be reproduced and the corresponding synergy inputs (q_{1i} and q_{2i}) are designated in Fig. 3(b). The errors associated with the reproduced postures $\tilde{\mathbf{j}}_i$ can be quantified according to Eq. (5). An overall hand reconstruction error, which is defined as in Eq. (18), is 21.10°.

$$\xi = \frac{\sum_{i=1}^{N} ||\mathbf{j}_i^{\mathrm{err}}||}{N}. \tag{18}$$

Then the posture matrix $\mathbf{J}_2$ is formed by expanding $\mathbf{J}_1$ with the six hand postures from the Set-2. The singular values are obtained and they are also plotted in Fig. 3(a). The biggest two singular values are now 187.36 and 141.43, whereas the synergy ratio η decreases to 72.29%. With the new posture matrix $\mathbf{J}_2$, a new synergy pair could be found and a new actuation zone (AZ-2) could be generated and overlaid in Fig. 3(b). Utilizing the new synergy pair, the 21 hand postures (15 from the Set-1 and six from the Set-2) can be reconstructed and the corresponding synergy inputs (q_{1i} and q_{2i}) are also designated in Fig. 3(b). Under these synergy inputs, the overall hand reconstruction error is now increased to 29.80°.

When $\mathbf{J}_2$ is further expanded with the 10 hand postures from the Set-3 to form the posture matrix $\mathbf{J}_3$, among the singular values plotted in Fig. 3(a), the biggest two singular values are now 338.46 and 239.74 and the synergy ratio η further decreases to 65.65%. With the updated synergy pair extracted from the posture matrix $\mathbf{J}_3$, an updated actuation zone (AZ-3) is overlaid in Fig. 3(b). To be noted, now the AZ-3 does not include all the hand postures. Many postures in the Set-3, whose joint angles are at the joint limits, lead to the points in the synergy plane outside the AZ-3. Then an optimization could be formulated as in Eq. (19) for the calculation of the synergy inputs (q_{1i} and q_{2i}) so that the reconstruction errors are to be minimized. These new points are designated as Set-3′ in Fig. 3(b). Counting all the points within the AZ-3, the overall hand reconstruction error is now further increased to 66.00°.

$$\min_{q_{1i}, q_{2i} \in \text{Actuation Zone}} \quad ||\mathbf{j}_i - \bar{\mathbf{j}} - q_{1i}\mathbf{u}_1 - q_{2i}\mathbf{u}_2||. \tag{19}$$

It can be clearly seen from the results above that the first two singular values become less dominant for more dissimilar hand postures and the posture reconstruction errors are increased. As shown in Fig. 3(c), the reproduced hand postures for the cup grasping (using synergies from $\mathbf{J}_1$, $\mathbf{J}_2$ and $\mathbf{J}_3$) deviate more and more severely from the original posture as shown in Fig. 2(b). The choice of the cup grasp is only for example. The same tend was also observed for other grasp postures. The norm of the hand reconstruction error $||\mathbf{j}_i^{\mathrm{err}}||$ is 8.99°, 31.01° and 48.02°, respectively. It is obvious that the linear method becomes particularly ineffective to handle distinct hand postures.

These results are also summarized in Table 2.

Table 2. Comparison of the posture reconstruction errors.

	Overall hand reconstruction error (°)			Reconstruction error for cup grasp (°)		
	$\mathbf{J}_1$	$\mathbf{J}_2$	$\mathbf{J}_3$	$\mathbf{J}_1$	$\mathbf{J}_2$	$\mathbf{J}_3$
Linear synergies	21.10°	29.80°	66.00°	8.99°	31.01°	48.02°
Nonlinear synergies	10.12°	13.76°	17.31°	2.75°	4.85°	27.63°
Error reduction	52.04%	53.83%	73.77%	69.41%	84.36%	42.46%

On the other hand, the nonlinear synergy synthesis constructs a mapping between the hand posture space and the latent space. Intrinsic structure of this mapping would vary with respect to the level of the hand posture dissimilarity. Such a method is hence ideal for the handling of distinct hand postures.

The latent space for the nonlinear synergy synthesis shown in Fig. 4 heavily depends on the observed data (the measured postures). Ideally, more hand postures shall be recorded for the synthesis. In order to keep the comparison consistent, the nonlinear synthesis still primarily uses the hand postures from the Set-1, Set-2 and Set-3. To increase the number of the hand postures, interpolation between these hand postures are included. The reason for this interpolation is as follows: The interpolated hand postures are all within the hand motion capability, since 13 motors drive this hand. Hence the likelihood of achieving these postures should be high. If the interpolated postures are excluded, it will lead to deviated results in the likelihood optimization for $p(\overleftrightarrow{\mathbf{J}})$ from Eq. (9). Only with the interpolated postures, the latent space in Fig. 4 properly indicates the hand motion capabilities from the collected posture sets.

While synthesizing the nonlinear synergy for the Set-1, any two hand postures are interpolated to generate three more hand postures for the synthesis according to

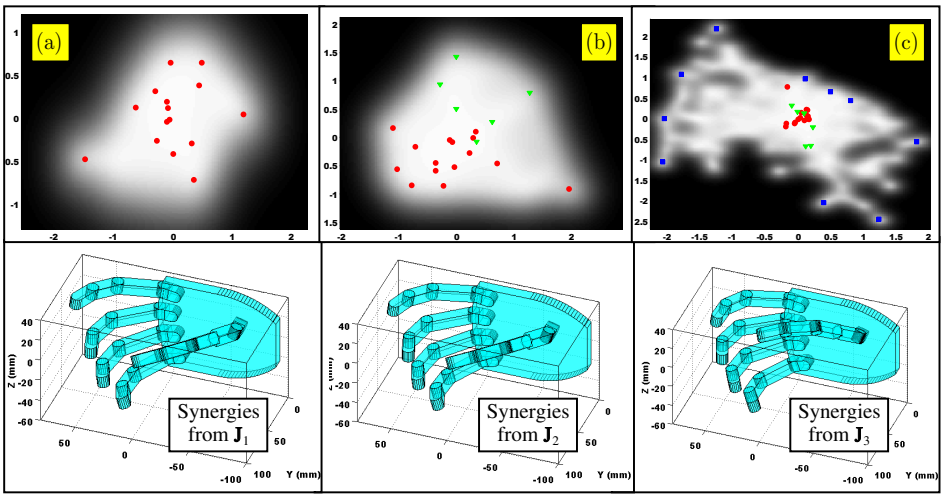

Fig. 4. Postural synergy synthesis using the nonlinear GPLVM method: the latent space with reproduced cup grasping postures for (a) the Set-1, (b) the Set-1 and Set-2 and (c) the Set-1, Set-2 and Set-3.

Eq. (20). Then, the total number of the hand postures are increased to $C_{15}^2 \times 3 + 15 = 330$.

$$\mathbf{j}_n = \frac{n}{4}\mathbf{j}_i + \frac{4-n}{4}\mathbf{j}_j, \quad n = 1, 2, 3 \quad \text{and} \quad i, j = 1, 2, \ldots, N. \tag{20}$$

Using these postures, the latent space could be plotted as in Fig. 4(a) with the original 15 postures in the Set-1 designated. The latent place does not have an explicit physical meaning. Hence the axes are not marked with a unit. The postures could now be reconstructed according to Eq. (13) and the overall hand reconstruction error defined as in Eq. (18) is 10.12°. For the calculation of the overall hand reconstruction error, the interpolated postures are excluded.

When the hand postures in the Set-2 are included, the synthesis could be carried out similarly. The same interpolation technique was applied and the total number of the hand postures are increased to $C_{21}^2 \times 3 + 21 = 651$. Using these postures, the latent space could be plotted as in Fig. 4(b) with the original postures in the Set-1 and Set-2 designated. The overall hand reconstruction error is now 13.76°.

When the hand postures in the Set-3 are further included, the total number of the hand postures are increased to $C_{31}^2 \times 3 + 31 = 1426$. The latent space is plotted as in Fig. 4(c) with the original postures designated. The overall hand reconstruction error is now slightly increased to 17.31°.

Compared to the results from the linear synthesis, the overall hand reconstruction error is reduced by 52.04%, 53.83% and 73.77%, respectively.

As shown in Fig. 4, the hand postures for the cup grasping now deviate less from the original posture as shown in Fig. 2(b). The norm of the hand reconstruction error $||\mathbf{j}_i^{\text{err}}||$ is only 2.75°, 4.85° and 27.63°, respectively.

These results are also summarized in Table 2.

The essential reason for these improvements is that the intrinsic structure of this GPLVM nonlinear mapping would vary with respect to the level of the hand posture dissimilarity. The latent space is expanded from the one in Fig. 4(a) to the one in Fig. 4(c) when more dissimilar hand postures are included. On the contrary, the ranges of the actuation zones generated during the linear synthesis remain relatively similar as shown in Fig. 3(b). When the hand postures become more dissimilar, this linear synthesis becomes less capable in reproducing the hand postures.

4.2. *Reproduction of hand postures*

The results obtained in Sec. 4.1 are further verified in this section on the actual prosthetic hand from Fig. 2(a).

As elaborated in Sec. 2, a desktop PC is used to generate the actuator trajectories and the trajectories are sent to the control workstation via UDP to drive the hand.

To reproduce a hand posture (e.g., the cup-grasping posture) via the linear postural synergies, the corresponding synergy inputs (q_{1i} and q_{2i}) are used to calculate the hand posture according to Eq. (4). Then, the joint trajectories are generated by linearly interpolating the joint angles between the target posture and the current

posture so that the hand postures could be smoothly changed. Each joint of the hand would follow the trajectories to form the target hand posture under the control of the servo system described in Sec. 2.

The posture reconstruction via nonlinear postural synergies is very similar except that the calculation of the target posture should refer to Eq. (13) instead.

The prosthetic hand was commanded to pose for (i) the cup-grasping posture, (ii) the ball-rotating posture P12 and (iii) the gesture for two as shown in Fig. 5. The linear synergies are obtained based on the posture matrix $\mathbf{J}_3$, while the nonlinear

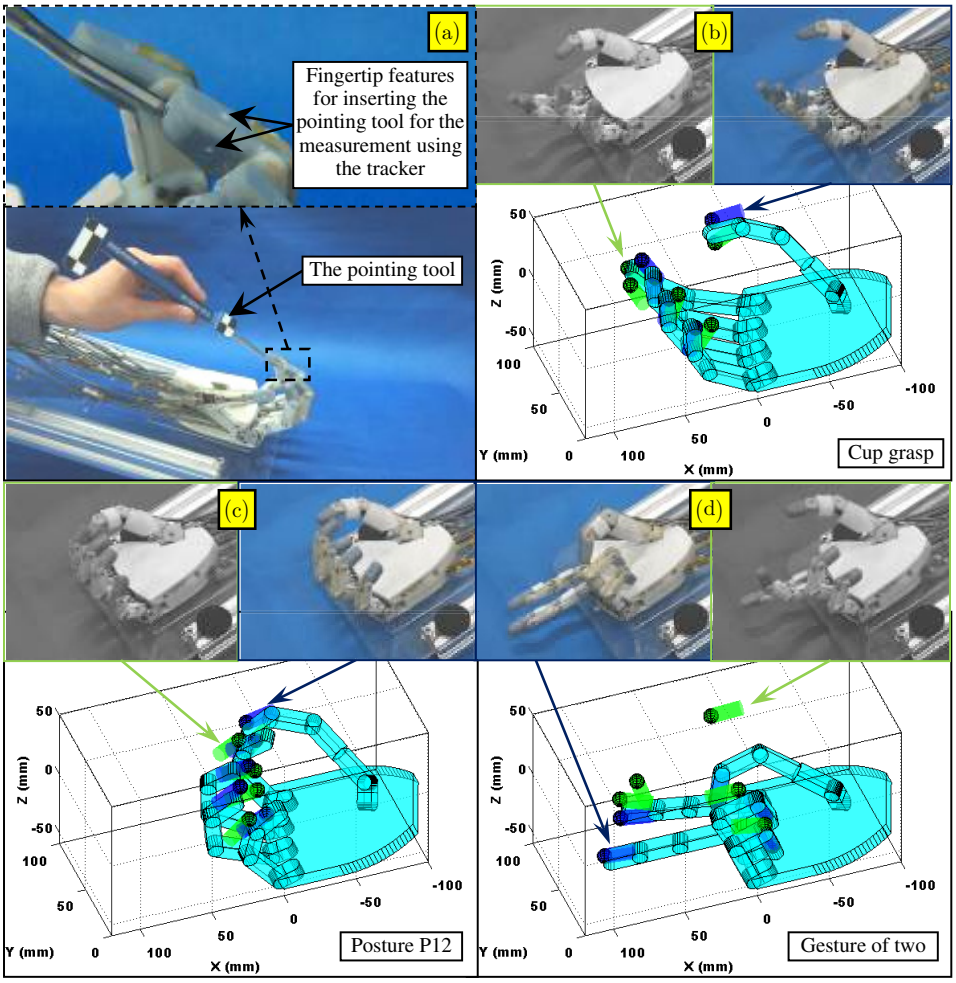

Fig. 5. Hand postures reproduced on the actual prosthetic hand: (a) Measurement using a tracker and fingertip comparisons between the desired and the reproduced postures for (b) the cup grasp, (c) the posture P12 and (d) the gesture of two. Grey photos are for the postures reproduced using the linear synergies (corresponding to green fingertips), while the colored ones are for those reproduced using the nonlinear synergies.

synergies are from Fig. 4(c). The selection of these hand postures from the Set-1, Set-2 and Set-3 is simply demonstrative. Other postures in the sets would show similar results.

Comparing to the original hand postures in Fig. 2, there are clear discrepancies between the original and the reproduced postures. The discrepancies were quantified using an optical tracker (Micron Tracker SX60, Claron Technology Inc.). As shown in Fig. 5, several holes with known positions and axes directions were reserved in the fingertips. The pointing tool was inserted into these holes one after another. The tip position and orientation of the pointing tool were read using the optical tracker. Then, the positions and orientations of the fingertips were identified using those of the pointing tool. The desired hand postures could be obtained from the realized synergies and the kinematic parameters of the hand. The actual (spherical fingertips) and the desired (cylindrical fingertips) are visualized in Fig. 5 accordingly. View angles of these plots are set so for the consistency with the hand photos. The green cylindrical fingertips are for the actual hand postures reproduced using the linear synergies, while the blue cylindrical ones are for those reproduced using the nonlinear synergies.

For the hand postures reproduced using the linear synergies, the position errors range from 4.80 mm to 78.24 mm and the orientation errors range from 6.88° to 94.59°. The average position error is 26.29 mm while the average orientation error is 36.37°.

For the hand postures reproduced using the nonlinear synergies, the position errors range from 3.26 mm to 34.89 mm and the orientation errors range from 2.74° to 13.56°. The average position error is 9.14 mm while the average orientation error is 7.83°. The average position error is reduced by 65.23% and the average orientation error is reduced by 78.47% while compared to the posture reproduction results using the linear synergies.

Two aspects mainly contribute to these errors: (i) the errors introduced by the synergies and (ii) the errors stemmed from the manufacturing tolerances, assembly errors and backlashes in the mechanical structures of the hand. Since the same hand was used while the linear synergies led to bigger errors, the experiments confirmed that the nonlinear synergies worked better in reproducing a wide spectrum of distinct hand postures.

To be noted, the experiments shown in Fig. 5 only describe whether a hand posture could be reproduced to a certain level of precision using the linear or the nonlinear synergies. Since the hand is not equipped with tactile sensors on the finger tips, it is not trivial to tell whether a form-closed or a force-closed grasp could be established. Grasping capabilities of these postures are investigated in the next section.

4.3. *Grasping of daily-life objects*

The quantification of the posture errors in Sec. 4.2 is not equivalent to an evaluation of the grasping capabilities of the prosthetic hand that deploys linear or nonlinear

postural synergies. Another set of experiments were hence carried out to examine the hand's grasping capabilities.

The 15 grasping postures of the daily-life objects from Set-1 were first reproduced. The synergy inputs (q_{1i} and q_{2i}) were used to calculate the hand postures according to Eqs. (4) or (13) for the linear and the nonlinear postural synergies, respectively. The linear synergies are obtained based on the posture matrix $\mathbf{J}_3$, while the nonlinear synergies are from Fig. 4(c). The control system drove the prosthetic hand to the reproduced postures.

Then, the synergy inputs were slightly adjusted around the original values to change the hand postures around the reproduced ones. The adjusted hand postures were examined to verify whether the daily-life objects could be grasped. Some of the reproduced and adjusted hand postures are shown in Fig. 6.

The adjustments (or optimization) of the inputs to the linear postural synergies for achieving stable grasps were investigated through analytical formulation in a milestone work.[29] A similar analytical investigation for the nonlinear postural synergies is also possible but out of the scope of this study. In this experiment, the adjustments of the synergy inputs were performed by a human operator, while the grasps were validated on the actual objects. It is similar to the scenario where an amputee tries to use this prosthetic hand for grasps.

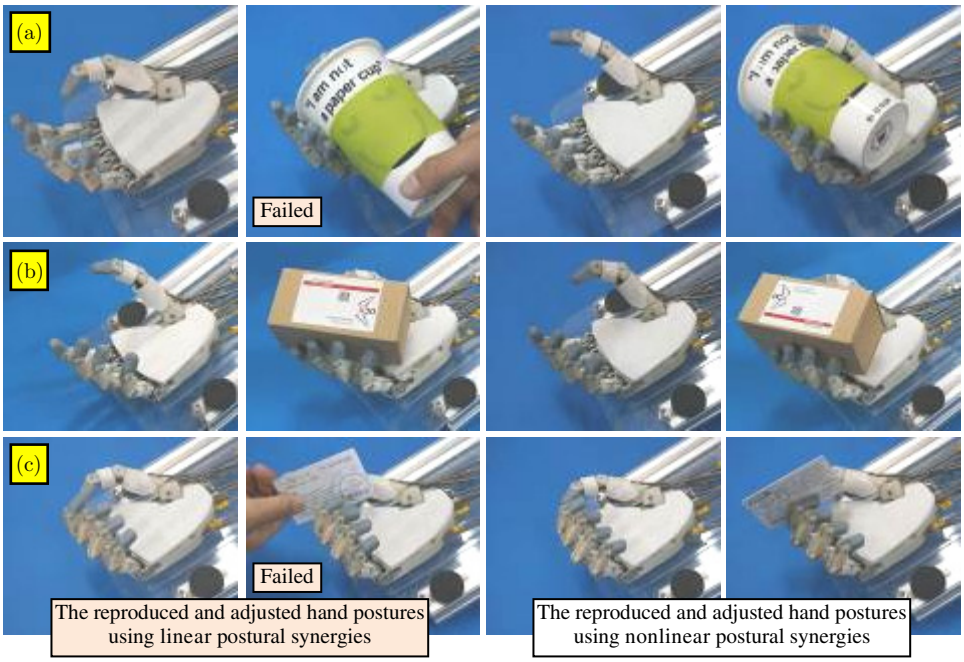

Fig. 6. Hand postures are adjusted to examine the grasping capabilities: (a) The cup grasp, (b) the tennis ball grasp and (c) the credit card grasp.

Table 3. Comparison of the hand posture adjustments for the grasps of daily-life objects.

#	Grasps	Linear synergies			Nonlinear synergies			Adjustment comparison ratio (%)
		Original inputs	Adjusted inputs	Normalized variation	Original inputs	Adjusted inputs	Normalized variation	
1	CD	12.2,−32.8	35.1,−16.3	0.067	−0.20,−0.19	−0.23,−0.22	0.007	10.10
2	Cup	3.9,−39.9	—	—	−0.20,−0.12	−0.15,−0.05	0.014	—
3	Coca can	−8.9,−20.75	—	—	−0.06,−0.10	−0.02,−0.05	0.011	—
4	Spray can	−26.6,−11.9	−28.1,−5.0	0.017	−0.01,−0.02	−0.03,0.02	0.008	47.35
5	Phone	−68.0,−1.7	−65.1,15.0	0.040	0.13,0.21	0.03,0.18	0.019	47.21
6	Flat bottle	−60.3,3.0	−60.9,11.2	0.019	0.12,0.23	0.04,0.18	0.016	83.62
7	Box	−7.3,−31.9	−1.0,−23.3	0.026	−0.06,−0.11	−0.03,−0.18	0.013	52.22
8	Book	−40.7,−17.5	−30.1,−29.7	0.039	0.14,−0.01	0.05,−0.05	0.017	43.78
9	Tennis ball	0.0,−3.9	−24.8,5.2	0.062	0.02,0.027	−0.03,0.1	0.016	24.98
10	Jar	−39.4,−20.7	−20.0,−10.1	0.052	0.16,−0.02	0.13,0.02	0.008	14.96
11	Golf ball	−42.8,−2.8	−55.0,−15.1	0.041	0.12,0.08	0.25,0.10	0.024	59.36
12	Drug bottle	−44.4,−13.6	−49.6,−20.1	0.020	0.14,0.05	0.17,0.07	0.006	29.96
13	Pen	−33.9,−11.1	—	—	0.09,−0.05	0.01,−0.02	0.015	—
14	Credit card	−42.2,6.4	—	—	0.04,0.15	0.08,0.15	0.007	—
15	Screwdriver	−64.8,43.7	−50.1,30.3	0.048	−0.17,0.78	−0.18,0.85	0.013	26.55

As shown in Fig. 6(a), the reproduced grasp for the cup implementing the linear postural synergies could not be adjusted to achieve a proper grasp. On the other hand, the cup could be grasped by adjusting the synergy inputs to the nonlinear postural synergies. Similar results were obtained for the credit card grasp as shown in Fig. 6(c). Although adjustments of the inputs to both the linear and the nonlinear postural synergies led to grasps of the box in Fig. 2(b), less adjustment was performed for the case of the nonlinear postural synergies, as shown in Fig. 6(b).

The adjustments are summarized in Table 3. The grasps for (i) the cup, (ii) the coca can, (iii) the pen and (iv) the credit card cannot be formed no matter how the synergy inputs were adjusted, if the linear postural synergies were used. For other objects, adjustments in the synergy inputs led to acceptable grasps. Since the synergy inputs for the linear and nonlinear cases have different interpretations, the normalized variation was defined to quantify the adjustments. It is defined as the ratio of the norm of the adjusted inputs (Δq_{1i} and Δq_{2i}) over a characteristic length. The characteristic lengths for the linear and the nonlinear cases are the diagonal lengths of the plotting areas of Figs. 3(b) and 4(c), respectively. Then, the adjustment comparison ratio is defined as the ratio of the normalized variation of the nonlinear case over the linear case. From Table 3, the average of the adjustment comparison ratio is 40.01%, excluding the four cases where the linear postural synergies could not be used to form feasible grasps. This indicates that only two-fifth of the adjustments are needed to form a proper grasp with the nonlinear postural synergies, if the grasps can be formed at all.

To be noted, the failed grasps in Fig. 6 are due to the use of the particular linear synergies extracted the posture matrix $\mathbf{J}_3$. If the linear synergies are subject to further optimizations, it is still possible to achieve proper grasps of these objects.

5. Conclusion

This paper presents a comparative study for postural synergy synthesis using a PCA-based linear method and a GPLVM-based nonlinear method.

Upon the construction of a 13-DoF anthropomorphic prosthetic hand and the collection of a comprehensive set of hand postures, implementations of the linear and nonlinear postural synergy syntheses are elaborated.

Inputs to the linear synergies could be interpreted as the coefficients while combining the synergies. Bio-signals (e.g., EMG) from an amputee could be directly used as the inputs. Although the synthesized nonlinear postural synergies no longer have explicit forms and the inputs do not have explicit physical meanings neither, it is still attainable to map two channels of bio-signals to the thirteen-dimensional hand posture via the synthesized nonlinear synergies.

In the numerical simulations, all the hand postures were reconstructed using the linear and the nonlinear synergies according to the corresponding synergy inputs. The overall hand reconstruction error using the nonlinear synergies is reduced by up

to 73.77% for different posture sets, while compared to the posture reproduction results using the linear synergies.

The superiority of the nonlinear synergies was further confirmed by the experimental validations on the actual prosthetic hand. The average fingertip position error is reduced by 65.23% and the average orientation error is reduced by 78.47%, while using the nonlinear synergies. When the postures only include daily-object grasps, although the linear synergies lead to acceptable results, the advantage of the nonlinear synergies is already obvious since the posture reconstruction error is 10.12° versus 21.10°. When the postures become more dissimilar, only the nonlinear synthesis could manage to generate acceptable results. What is more, an amputee could adjust the hand postures to achieve proper grasps of daily-life objects more easily when the nonlinear postural synergies are used. The adjustment is 40.01% of the case of the linear postural synergies.

The presented results revealed the potentials of nonlinear postural synergies. It is suggested that the use of nonlinear postural synergies should be considered while applying a multi-DoF dexterous robotic hand as prosthesis. Although the implementation of nonlinear synergies is somehow complicated, it makes full use of the computational power of a modern controller and could drive a multi-DoF hand to reproduce versatile hand postures more precisely via only two channels of bio-signals.

Acknowledgments

This work is supported in part by the National Program on Key Basic Research Projects (Grant No. 2011CB013300), in part by the Science and Technology Commission of Shanghai Municipality (Grant No. 13430721600) and in part by the National Natural Science Foundation of China (Grant No. 51375296).

References

1. N. Bernstein, The problem of the interrelation of coordination and localization, *Arch. Biol. Sci.* **38**(1) (1935) 1–34.
2. M. Santello, M. Flanders and J. F. Soechting, Postural hand synergies for tool use, *J. Neurosci.* **18**(23) (1998) 10105–10115.
3. J. R. Napier, The prehensile movements of the human hand, *J. Bone Joint Surg.* **38**(4) (1956) 902–913.
4. M. R. Cutkosky, On grasp choice, grasp models, and the design of hands for manufacturing tasks, *IEEE Trans. Robot. Autom.* **5**(3) (1989) 269–279.
5. T. Feix, R. Pawlik, H.-B. Schmiedmayer, J. Romero and D. Kragiæ, A comprehensive grasp taxonomy, in *Robotics, Science and Systems Conf. (RSS)*, Seattle, Washington, USA, 2009, pp.
6. J. Z. Zheng, S. De La Rosa and A. M. Dollar, An investigation of grasp type and frequency in daily household and machine shop tasks, *IEEE Int. Conf. Robotics and Automation (ICRA)*, Shanghai, China, 2011, pp. 4169–4175.
7. H. Liu, P. Meusel, N. Seitz, B. Willberg, G. Hirzinger, M. H. Jin, Y. W. Liu, R. Wei and Z. W. Xie, The modular multisensory DLR-HIT-hand, *Mech. Mach. Theory* **42**(5) (2007) 612–625.

8. M. Grebenstein, M. Chalon, W. Friedl, S. Haddadin, T. Wimböck, G. Hirzinger and R. Siegwart, The hand of the DLR hand arm system: Designed for interaction, *Int. J. Robot. Res.* **31**(13) (2012) 1531–1555.
9. M. Quigley, C. Salisbury, A. Y. Ng and J. K. Salisbury, Mechatronic design of an integrated robotic hand, *Int. J. Robot. Res.* **33**(5) (2014) 706–720.
10. T. Wimböck, B. Jahn and G. Hirzinger, Synergy level impedance control for multifingered hands, *IEEE/RSJ Int. Conf. Intelligent Robots and Systems (IROS)*, San Francisco, CA, USA, 2011, pp. 973–979.
11. J. Rosell, R. Suárez, C. Rosales and A. Pérez, Autonomous motion planning of a hand-arm robotic system based on captured human-like hand postures, *Auton. Robots* **31**(1) (2011) 87–102.
12. F. Ficuciello, G. Palli, C. Melchiorri and B. Siciliano, Experimental evaluation of postural synergies during reach to grasp with the UB hand IV, *IEEE/RSJ Int. Conf. Intelligent Robots and Systems (IROS)*, San Francisco, CA, USA, 2011, pp. 1775–1780.
13. E. Rombokas, M. Malhotra and Y. Matsuoka, Task-specific demonstration and practiced synergies for writing with the act hand, *IEEE Int. Conf. Robotics and Automation (ICRA)*, Shanghai, China, 2011, pp. 5363–5368.
14. A. Zhang, M. Malhotra and Y. Matsuoka, Musical piano performance by the ACT hand, *IEEE Int. Conf. Robotics and Automation (ICRA)*, Shanghai, China, 2011, pp. 3536–3541.
15. A. Bicchi, M. Gabiccini and M. Santello, Modelling natural and artificial hands with synergies, *Philos. Trans. R. Soc. B, Biol. Sci.* **366**(1581) (2011) 3153–3161.
16. G. Palli, C. Melchiorri, G. Vassura, U. Scarcia, L. Moriello, G. Berselli, A. Cavallo, G. D. Maria, C. Natale, S. Pirozzi, C. May, F. Ficuciello and B. Siciliano, The DEXMART hand: Mechatronic design and experimental evaluation of synergy-based control for human-like grasping, *Int. J. Robot. Res.* **33**(5) (2014) 799–824.
17. C. Y. Brown and H. H. Asada, Inter-finger coordination and postural synergies in robot hands via mechanical implementation of principal components analysis, *IEEE/RSJ Int. Conf. Intelligent Robots and Systems (IROS)*, San Diego, CA, USA, 2007, pp. 2877–2882.
18. W. Chen, C. Xiong and S. Yue, Mechanical implementation of kinematic synergy for continual grasping generation of anthropomorphic hand, *IEEE/ASME Trans. Mechatronics* **20**(3) (2015) 1249–1263.
19. S. Li, X. Sheng, H. Liu and X. Zhu, Design of a myoelectric prosthetic hand implementing postural synergy mechanically, *Ind. Robot, Int. J.* **41**(5) (2014) 447–455.
20. M. G. Catalano, G. Grioli, E. Farnioli, A. Serio, C. Piazza and A. Bicchi, Adaptive synergies for the design and control of the Pisa/IIT SoftHand, *Int. J. Robot. Res.* **33**(5) (2014) 768–782.
21. K. Xu, Y. Du, H. Liu, X. Sheng and X. Zhu, Mechanical implementation of postural synergies of an underactuated prosthetic hand, *Int. Conf. Intelligent Robotics and Applications (ICIRA)*, Busan, Korea, 2013, pp. 463–474.
22. K. Xu, H. Liu, Y. Du and X. Zhu, Design of an underactuated anthropomorphic hand with mechanically implemented postural synergies, *Adv. Robot.* **28**(21) (2014) 1459–1474.
23. K. Xu, H. Liu, Y. Du, X. Sheng and X. Zhu, Mechanical implementation of postural synergies using a simple continuum mechanism, *IEEE Int. Conf. Robotics and Automation (ICRA)*, Hong Kong, China, 2014, pp. 1348–1353.
24. M. C. Carrozza, G. Cappiello, S. Micera, B. B. Edin, L. Beccai and C. Cipriani, Design of a cybernetic hand for perception and action, *Biol. Cybernet.* **95**(6) (2006) 629–644.
25. C. Gosselin, F. Pelletier and T. Laliberté, An anthropomorphic underactuated robotic hand with 15 Dofs and a single actuator, *IEEE Int. Conf. Robotics and Automation (ICRA)*, Pasadena, CA, USA, 2008, pp. 749–754.

26. S. A. Dalley, T. E. Wiste, T. J. Withrow and M. Goldfarb, Design of a multifunctional anthropomorphic prosthetic hand with extrinsic actuation, *IEEE/ASME Trans. Mechatronics* **14**(6) (2009) 699–706.
27. C. Cipriani, M. Controzzi and M. C. Carrozza, Objectives, criteria and methods for the design of the SmartHand transradial prosthesis, *Robotica* **28**(6) (2010) 919–927.
28. M. T. Ciocarlie, C. Goldfeder and P. K. Allen, Dexterous grasping via eigengrasps: A low-dimensional approach to a high-complexity problem, in *Robotics: Science and Systems*, Atlanta, Georgia, USA, 2007, pp.
29. M. T. Ciocarlie and P. K. Allen, Hand posture subspaces for dexterous robotic grasping, *Int. J. Robot. Res.* **28**(7) (2009) 851–867.
30. T. Feix, J. Romero, C. H. Ek, H.-B. Schmiedmayer and D. Kragic, A metric for comparing the anthropomorphic motion capability of artificial hands, *IEEE Trans. Robot.* **29**(1) (2013) 82–93.
31. J. Romero, T. Feix, C. H. Ek, H. Kjellström and D. Kragic, Extracting postural synergies for robotic grasping, *IEEE Trans. Robot.* **29**(6) (2013) 1342–1352.
32. H. Huang, L. Jiang, Y. Liu, L. Hou, H. Cai and H. Liu, The mechanical design and experiments of HIT/DLR prosthetic hand, *IEEE Int. Conf. Robotics and Biomimetics (ROBIO)*, Kunming, China, 2006, pp. 896–901.
33. E. J. Weiss and M. Flanders, Muscular and postural synergies of the human hand, *J. Neurophysiol.* **92**(1) (2004) 523–535.
34. N. Lawrence, Probabilistic non-linear principal component analysis with Gaussian process latent variable models, *J. Mach. Learn. Res.* **6** (2005) 1783–1816.
35. N. D. Lawrence and J. Quiñonero-Candela, Local distance preservation in the GP-LVM through back constrains, *Int. Conf. Machine Learning (ICML)*, Pittsburgh, PA, USA, 2006, pp. 513–520.
36. N. Andrei, Scaled conjugate gradient algorithms for unconstrained optimization, *Comput. Optim. Appl.* **38**(3) (2007) 401–416.

AQ: Please provide page range for reference 5 and 28.

Kai Xu received the B. E. and M. S. degrees from the Department of Precision Instruments and Mechanology, Tsinghua University, Beijing, China, in 2001 and 2004, respectively, and the Ph.D. degree (with distinction) from the Department of Mechanical Engineering, Columbia University, New York, NY, in 2009. Since 2010, he has been with the University of Michigan — Shanghai Jiao Tong University Joint Institute, Shanghai Jiao Tong University, Shanghai, China, where he is currently an Associate Professor and the Director of the Robotics Innovation and Intervention Laboratory. His research interests include surgical robots, exoskeletons, humanoid robots, prosthetic hands, special industrial robots and continuum mechanisms.

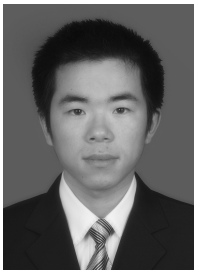

Huan Liu received the B. S. degree from the School of Mechanical Engineering, Huazhong Agricultural University, Wuhan, China, in 2008, and the M. S. degree from the School of Power and Mechanical Engineering, Wuhan University, Wuhan, China, in 2010. He is currently pursuing his Ph.D. degree in the University of Michigan — Shanghai Jiao Tong University Joint Institute, Shanghai Jiao Tong University, Shanghai, China. His research interests include prosthetic hands and biomechatronics.

Yuheng Du received the B. S. degree from the University of Michigan — Shanghai Jiao Tong University Joint Institute, Shanghai Jiao Tong University, Shanghai, China in 2013. He is currently pursuing his M. S. degree in the same institute.

Xiangyang Zhu received the B. S. degree from the Department of Automatic Control Engineering, Nanjing Institute of Technology, Nanjing, China, in 1985, the M.Phil. degree in instrumentation engineering and the Ph.D. degree in automatic control engineering, both from Southeast University, Nanjing, China, in 1989 and 1992, respectively. From 1993 to 1994, he was a Postdoctoral research fellow with Huazhong University of Science and Technology, Wuhan, China. He joined as an associate professor in the Department of Mechanical Engineering, Southeast University, in 1995. Since June 2002, he has been with the School of Mechanical Engineering, Shanghai Jiao Tong University, Shanghai, China, where he is currently a Changjiang Chair Professor and the Director of the Robotics Institute. His current research interests include robotic manipulation planning, human–machine interfacing and biomechatronics. Dr. Zhu received the National Science Fund for Distinguished Young Scholars in 2005.